# THEORETICAL ANALYSIS OF UNSTEADY BLADE LOADING OF INDUCERS UNDER ROTATING CAVITATION

**S. Watanabe, A. Furukawa**
Kyushu University, Fukuoka, Japan
**H. Horiguchi, J. Fukutomi**
Tokushima University, Tokushima, Japan
**and Y. Tsujimoto**
Osaka University, Toyonaka, Japan

## Abstract

Rotating cavitation is one of the flow instabilities associated with cavitation, which has been a problem for the development of turbopumps of liquid rocket engines since it causes super-synchronous shaft vibration. Recently, it is argued that rotating cavitation might also cause large repetitive stresses on blades. This paper describes about the theoretical prediction of unsteady blade forces on the cavitating inducer under rotating cavitation. Unsteady pressure distributions and a lift force for a 2-dimensitional flat plate cascade under rotating cavitation are calculated by using a linearized free streamline theory based on the unsteady closed cavity model and singularity method. Since the linearized calculation cannot predict the absolute magnitude of the fluctuations, the unsteady pressure distributions and resulting lift fluctuations are presented for a given magnitude of cavity length fluctuations.

## 1. Introduction

Rotating cavitation is one of the most important problems for the development of high-speed turbopumps for rocket engines. Under rotating cavitation, turbopumps often suffer from supersynchronous shaft vibration (Kamijo et al. 1993; Tsujimoto et al., 1997). Moreover, it is recently argued that the pressure fluctuation caused by rotating cavitation may induce a significant blede stress (Maekawa et al., 1997). So, it is important to construct the reliable method to predict the unsteady blade loadings.

The efforts to understand the mechanism of rotating cavitation have been made by theoretical works such as Tsujimoto et al. (1993), Watanabe et al. (1999), and so on. From their results, many types of rotating cavitation are theoretically predicted, including conventional forward rotating cavitation, backward rotating cavitation, and higher order rotating cavitations.

In the present study, a theoretical method to predict unsteady pressure distributions and a lift force for a 2-dimensitional flat plate cascade under rotating cavitation is described. The method is constructed based on the linearized free streamline theory (Furuya, 1982) combining the unsteady closed cavity model and singularity method.

## 2. Outline of Analysis

### 2.1. Stability analysis of fundamental flow field

We analyze a flow through a flat plate cascade with the chord length of $C$, the spacing of $h$, and the stagger of $\beta$, as shown in Figure 1. We assume a main flow of magnitude $U$ and the incidence angle $\alpha$ at upstream infinity. We define the index of blades $n$ by taking into account the periodicity for an inducer with blade number $Z_N$: The blade on the $x$-axis is given the index zero, and the index increases in the positive direction of the $y$-axis and returns to zero at the $Z_N$th blade. We consider the case of partial cavitation and assume small disturbances with time dependence $\exp(j\omega t)$ , in which $\omega=\omega_R+j\omega_I$ is a complex angular frequency with the angular frequency of $\omega_R$ and the decay rate of $\omega_I$, to be determined from the analysis. By assuming the interblade phase difference of disturbances, $\Delta\varphi=2\pi m/Z_N$ ($m$: number

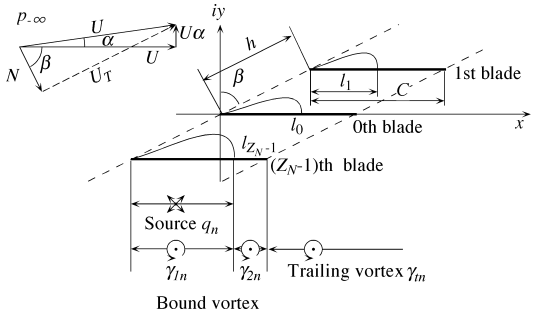


Figure 1: Model for present analysis

of cells), we can simulate the circumferential propagation of fluctuations in rotating cavitation.

The flow disturbance due to the existence of blades and cavities is represented by a source distribution $q_n$ on the cavitating region, vortex distributions $\gamma_{1n}$ and $\gamma_{2n}$ along the blades, and a trailing free vortex distribution $\gamma_{tn}$ along the wake surface of the blades. The strengths of these singularities are defined on the coordinate fixed to the cavity to take account of the cavity length fluctuation. Dividing the strength of singularities and the cavity length into steady and unsteady components, we can represent the velocity with the steady uniform velocity ($U$, $U\alpha$), the steady disturbance ($u_s$, $v_s$), and the unsteady disturbance ($\tilde{u}, \tilde{v}$ ) as follows:

$$\begin{aligned} u &= U + u_s + \tilde{u}\exp(j\omega t) \\ v &= U\alpha + v_s + \tilde{v}\exp(j\omega t) \end{aligned} \tag{1}$$

We assume that $\alpha << 1, U >> |u_s|, |v_s| >> |\tilde{u}|, |\tilde{v}|$ and neglect higher order small terms.

The boundary and complementary conditions to determine the flow field are as follows:

(1) The pressure on the cavity should be equal to the vapor pressure ($p_v$).
(2) The normal velocity on the wetted blade surface should vanish.
(3) The cavity should close at the moving cavity trailing edge.
(4) The pressure difference across the blades should vanish at the trailing edge (unsteady Kutta's condition.)

By specifying the strength of singularities at the nodes ($S_{ij}$) on the coordinates fixed to the fluctuating cavity as unknowns, then dividing the above conditions into steady and unsteady parts, we can obtain the following linear equations;

For the steady component,

$$\begin{bmatrix} & & \\ & A_s(l_s) & \\ & & \end{bmatrix} \begin{Bmatrix} q_s(S_{11})/U\alpha \\ \vdots \\ \gamma_{1s}(S_{11})/U\alpha \\ \vdots \\ \gamma_{2s}(S_{21})/U\alpha \\ \vdots \\ \sigma/2\alpha \end{Bmatrix} = \begin{Bmatrix} & \\ B_s & \\ & \end{Bmatrix} \tag{2}$$

and for the unsteady component,

$$\begin{bmatrix} & & \\ & A_u(l_s, \omega) & \\ & & \end{bmatrix} \begin{Bmatrix} \tilde{q}(S_{11}) \\ \vdots \\ \tilde{\gamma}_1(S_{11}) \\ \vdots \\ \tilde{\gamma}_2(S_{21}) \\ \vdots \\ \tilde{u}_c \\ \alpha \cdot \tilde{l} \end{Bmatrix} = \begin{Bmatrix} & \\ 0 & \\ & \end{Bmatrix} \tag{3}$$

where $A_s(l_s)$ and $A_u(l_s, \omega)$ are coefficient matrices, $B_s$ a constant vector, $\tilde{u}_c$ the unsteady component of tangential velocity on the cavity surface, and $\sigma = 2(p_{-\infty} - p_v)/\rho U^2$ the cavitation number upstream. The steady flow can be determined from Equation (2), which shows that the steady cavity length $l_s$ is a function of $\sigma/2\alpha$. Equation (3) is a set of linear homogeneous equations. The determinant of the coefficient matrix should be zero

$$\left|A_u(l_s, \omega) = 0\right| \tag{4}$$

so that we have non-trivial solutions. The complex frequency $\omega$ is determined from this equation. This equation shows that the frequency $\omega_R$ and decay rate $\omega_I$ as well as possible mode of instability depends on the steady cavity length $l_s$, or equivalently on $\sigma/2\alpha$, once the geometry and other flow conditions are given.

The complex propagation velocity ratio $k$ in the relative frame fixed to the moving cascade and $k^*$ in the absolute frame is defined as the ratio of the propagating velocity of disturbance to the moving velocity of cascade $U_T$ [$=U\sin(\beta+\alpha)$] as follows.

$$k = k_R + jk_I = \frac{\dfrac{\omega/m}{2\pi} Z_N h}{U_T} \tag{5}$$

$$k^* = k_R^* + jk_I^* = (1 - k_R) + jk_I \tag{6}$$

where $k_R^*$ is the propagation velocity in the absolute frame, and if $k_R^* > 1$, the corresponding mode is the forward propagating mode. $k_I^*$ is the decay rate, and if $k_I^*$ is negative, the magnitudes of disturbance increase exponentially, meaning that the corresponding mode is unstable.

We have experienced in the previous study (Watanabe et al, 1999) that there are a lot of unstable modes in addition to the conventional rotating cavitation mode. In the present study, we focus mainly on the conventional rotating cavitation mode.

## 2.2. Calculation of unsteady fluid forces

After the determination of the eigen-value $\omega$ from Equation (4), we can determine the mode of the instability associated with $\omega$ as the eigen-vector of Equation (3). In the poresent linear analysis we cannot determine the absolute magnitude of the instability and the eigen vector provides only relative magnitude. Here we assume that the magnitude of cavity length fluctuation is given and the pressure and lift fluctuations are presented associated with the cavity length fluctuation.

Integrating the momentum equation applied on the suction and pressure side of the blade, then subtracting the one from the other, we can obtain the pressure difference distribution across the blade as follows.

For the cavitating region ($0<x<l$, $0<s_1<1$)

$$\begin{gathered}\Delta p(s_1) = \Delta p_s(s_1) + \Delta\tilde{p}(s_1)\exp(j\omega t) \\ \Delta p_s(s_1)/\rho = U\gamma_{1s}(s_1) \\ \Delta\tilde{p}(s_1)/\rho = U\tilde{\gamma}_1(s_1) - j\omega l_s\int_0^{s_1}\tilde{\gamma}_1(s_1')ds_1' - j\omega\tilde{l}\left[s_1\gamma_{1s}(s_1) - \int_0^{s_1}\gamma_{1s}(s_1')ds_1'\right]\end{gathered} \tag{7}$$

and for the non-cavitating region ($l<x<C$, $1<s_2<2$)

$$\begin{gathered}\Delta p(s_2) = \Delta p_s(s_2) + \Delta\tilde{p}(s_2)\exp(j\omega t) \\ \Delta p_s(s_2)/\rho = U\gamma_{2s}(s_2) \\ \Delta\tilde{p}(s_2)/\rho = U[\tilde{\gamma}_2(s_2) - \tilde{\gamma}_2(2)] - j\omega(C - l_s)\int_{s_2}^{2}\tilde{\gamma}_2(s_2')ds_2' - j\omega\tilde{l}\left[(2 - s_2)\gamma_{2s}(s_2) - \int_{s_2}^{2}\gamma_{2s}(s_2')ds_2'\right]\end{gathered} \tag{8}$$

Integrating the above pressure distributions over the blade, we can obtain the lift coefficient as follows.

$$\begin{gathered}C_L = L/\rho U^2 C = C_{Ls} + \tilde{C}_L\exp(j\omega t) \\ C_{Ls} = \left[\int_0^1\gamma_{1s}(s_1)l_s ds_1 + \int_1^2\gamma_{ss}(s_s)(C - l_s)ds_s\right]/CU \\ \tilde{C}_L = \frac{1}{CU}\left\{\int_0^1\left[1 + j\frac{\omega}{U}(C - l_s s_1)\right]\tilde{\gamma}_1(s_1)l_s ds_1 + \int_1^2\left[1 + j\frac{\omega}{U}(C - l_s)(2 - s_2)\right]\tilde{\gamma}_2(s_s)(C - l_s)ds_s\right. \\ \left. + \frac{\tilde{l}}{l_s}\int_0^1\left[1 + j\frac{\omega}{U}(C - 2l_s s_1)\right]\gamma_{1s}(s_1)l_s ds_1 - \frac{\tilde{l}}{C - l_s}\int_1^2\left[1 + j\frac{2\omega}{U}(C - l_s)(2 - s_2)\right]\gamma_{2s}(s_s)(C - l_s)ds_s\right\}\end{gathered} \tag{9}$$

# 3. Results and discussions

Numerical results are shown for a cascade with the solidity of $C/h$=2.6, the stagger of $\beta$=79.5[deg.], and the number of blades of $Z_N$=3, as the default case. The number of cells of $m$=1 and the incidence angle of $\alpha$=4.0[deg.] are selected. Figure 2 shows the result of steady analysis, as the plots of the cavitation number $\sigma$ and the steady lift coefficient $C_{Ls}$ against the steady cavity lengths $l_s$. As the cavitation number decreases, the cavity extends gradually at larger cavitation number, and then it extends rapidly once the cavity extends into the blade passage ($l_s$>$h$). The steady lift coefficient $C_{LS}$ is almost constant because of the large solidity.

### 3.1. Results of stability analysis and lift fluctuation

Figure 3 shows the propagation velocity ratio of conventional rotating cavitation obtained by the stability analysis and the unsteady lift coefficient under rotating cavitation. We can see from Figure 3(a) that the propagation velocity ratio $k_R^*$ approaches to unity as the cavity length $l_s/C$ increases. The ratio of the unsteady lift coefficient to the normalized cavity length fluctuation $\tilde{C}_L/(\tilde{l}/C)$ is plotted in the complex plane as shown in Figure 3(b). As the steady cavity length increases, the magnitude of $\tilde{C}_L/(\tilde{l}/C)$ increases, then takes the maximum value around $l_s/C$=0.4, and begins to decrease. All of the plots of $\tilde{C}_L/(\tilde{l}/C)$ are on the 4th quadrant of the complex plain, indicating the phase advance of the lift fluctuation to the cavity length fluctuation because of negative frequency $k_R$ in the relative frame.

### 3.2. Unsteady pressure fluctuation

Figure 4 shows the time histories of the pressure coefficient $C_p=(p-p_v)/\rho U^2$ on the suction and pressure surfaces of the

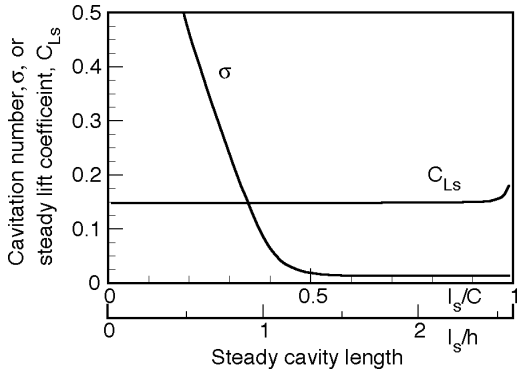


Figure 2: Steady cavity length and lift coefficient

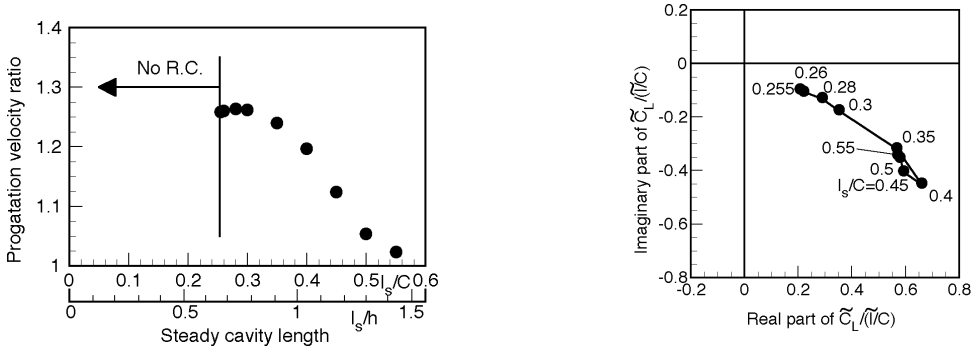


(a) Propagation velocity ratio (b) Unsteady lift coefficient

Figure 3: Propagation velocity ratio and unsteady lift coefficient

blade. Figure 4 (a) is for the neutrally stable case with the steady cavity length of $l_s/C$=0.255, and (b) is for the case with $l_s/C$=0.55 where the cavity extends into the blade passage deeply. The cavity length fluctuation with its magnitude of 10% of the steady cavity length is assumed for both cases. The angle $\theta=|\omega_R|t$ is the phase angle, and the cavity length takes its maximum value at $\theta$=0. The value of $x/C=h\sin\beta/C$ in the figures denotes the location of the leading edge of the opposing blade, showing that the blade passage starts there.

As we can see from Figure 4(a), the pressure distribution on the pressure surface does not change largely. The low pressure region on the suction surface fluctuates in accordance with the cavity length fluctuation and the large pressure fluctuation can be seen just downstream of the cavity trailing edge. This result might indicate that, for the case with shorter cavities, the pressure fluctuation on the suction surface is more responsible for the lift fluctuation.

On the other hand, as shown in Figure 4(b), when the cavity extends into the blade passage, the pressure fluctuation can be seen also on the pressure surface, especially around the leading edge. This is due to the cavity on the adjacent blade. This low pressure region on the pressure side is found to fluctuate in accordance with the cavity fluctuation on the adjacent blade, which means that the cavity behavior of the adjacent blade is also important for the lift fluctuation.

Figure 5 shows the unsteady components of the pressure distributions on the blade surfaces defined on the coordinate fixed to the cavity for the cases with the steady cavity lengths of $l_s/C$=0.255, 0.4 and 0.55. The values are normalized by the cavity length fluctuation. For the case with the shorter cavity [Figure 5(a)], the pressure fluctuation can be found only around the trailing edge of the cavity. However, as the cavity extends, the pressure fluctuation there becomes weak, and then the pressure around the blade leading edge on the pressure surface becomes to fluctuate, as shown in Figures 5 (b) and (c). This is because the low pressure region around the cavity on the adjacent blade approaches the leading edge of the pressure surface of the blade.

### 3.3. Quasi-static estimation of unsteady fluid forces

As we can see from the pressure distributions shown in Figure 4, it seems that the pressure difference across the blade in the cavitating region is the most responsible for the fluid force, because the pressure difference there are

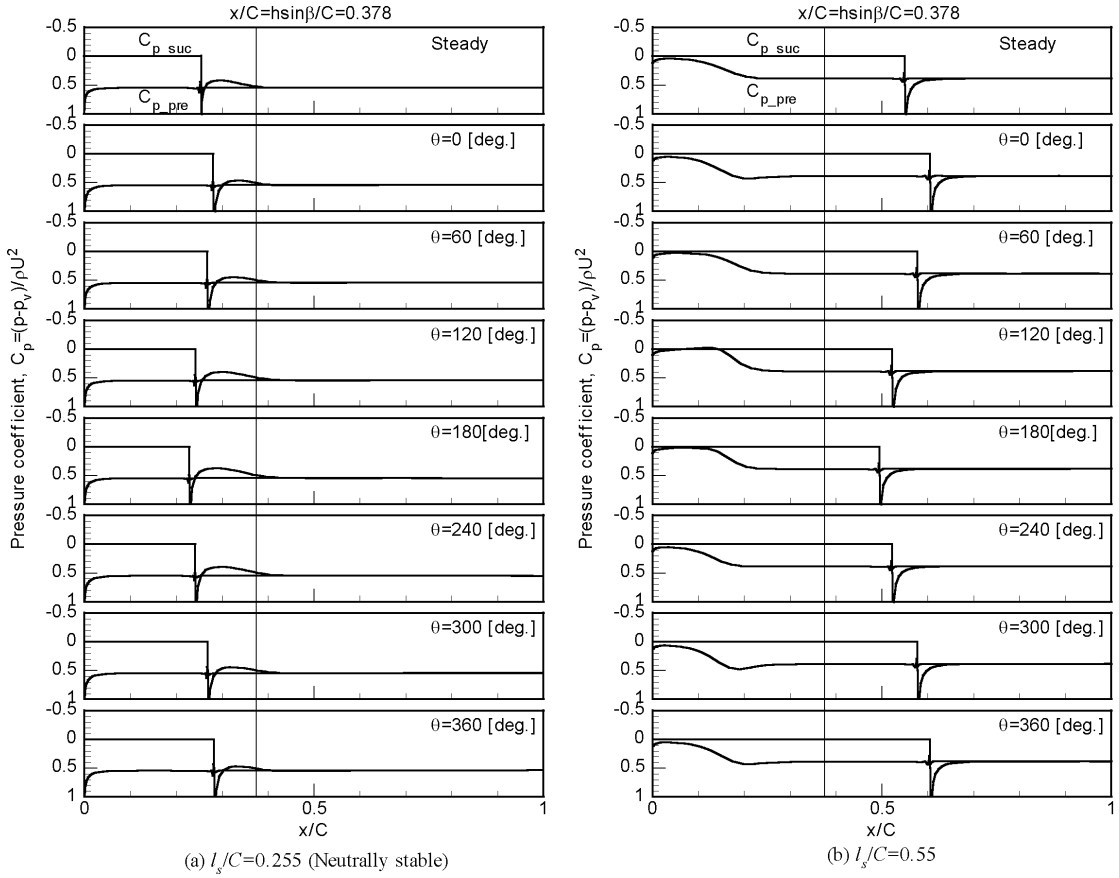


Figure 4: Time histories of pressure distributions along blade surfaces

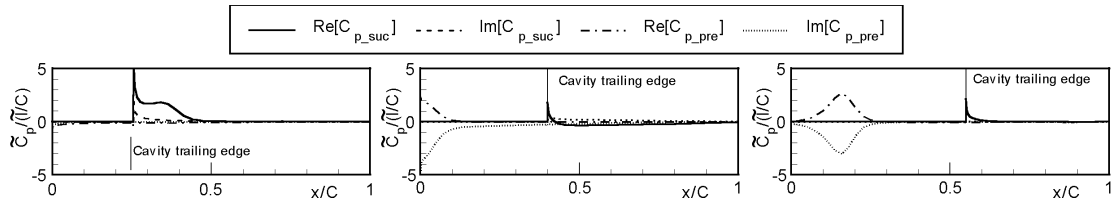


(a) $l_s/C$=0.25 (Neutrally stable) (b) $l_s/C$=0.4 (c) $l_s/C$=0.55

Figure 5: Unsteady pressure distributions

much larger than that in the other region. Here, we consider the quasi-static model for the estimation of the lift force as shown in Figure 6, based on the assumption in which the lift force can be calculated only from the pressure difference in the cavitating region. We also assume that only the area of the cavitating region changes whereas the pressure itself does not change at all.

For the case with shorter cavities as shown in Figure 6 (a), we can estimate the lift coefficient from the pressure difference $\Delta C_{pcavi}$ in the cavitating region and the cavity length as follows.

$$C_L \approx \Delta C_{pcavi}(l_s + \tilde{l}\, e^{j\omega t})/C = C_{Ls} + C_{Ls}\frac{C}{l_s}\cdot\frac{\tilde{l}}{C}\exp j\omega t \tag{10}$$

where the first term $C_{Ls} = \Delta C_{pcavi} l_s / C$ denotes the steady lift coefficient: the second term is the unsteady lift coefficient.

On the other hand, when the cavity extends into the blade passage, the pressure around the leading edge on the pressure surface is affected by the cavity of the adjacent blade as described above. Assuming that the pressure there equals to the vapor pressure, we can estimate the lift coefficient as follows, by considering the pressure difference only in the effective area $[l_n-(l_{n-1}-h)]$.

$$C_L \approx \Delta C_{pcavi}[(l_s + \tilde{l}\, e^{j\omega t}) - (l_s + \tilde{l}\, e^{j(\omega t+\Delta\varphi)} - h)]/C = C_{Ls} + C_{Ls}\frac{C}{h}\cdot(1-\exp j\Delta\varphi)\frac{\tilde{l}}{C}\exp j\omega t \tag{11}$$

where we should note that the steady lift coefficient can be expressed by $C_{Ls} = \Delta C_{pcavi} h / C$ .

Examples of the above quasi-static estimation of the lift coefficient fluctuation are shown in Table 1. The steady lift coefficients $C_{Ls}$ shown in Figure 2(a) are used for the quasi-static estimation. The unsteady lift coefficients obtained from Equation (9) are also shown in the table. We can see that, for the cases where the cavity extends into the blade passage ($l_s/C$=0.4 and 0.55), the quasi-static model can predict the unsteady lift force fairly well. Especially, for the case with $l_s/C$=0.55, very good agreement is obtained. This might indicate that, while the unsteady lift coefficient shows its unsteadiness as shown in Figure 2(b), we can predict it quasi-statically if we consider the influence of the cavity behavior on the adjacent blade. On the other hands, for the case of shorter cavity with

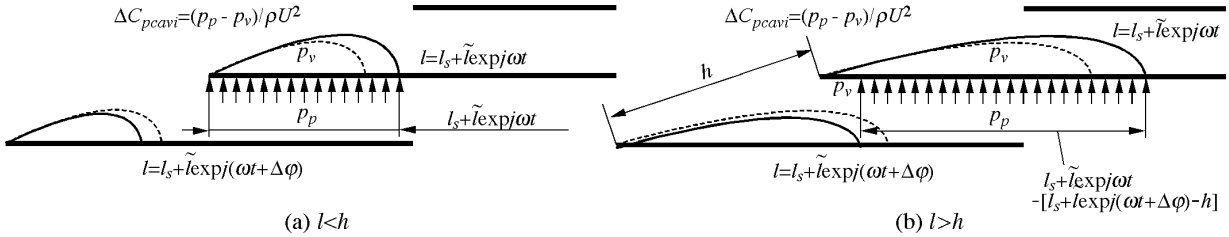


(a) $l<h$ (b) $l>h$

Figure 6: Quasi-static model for predicting lift coefficient

Table 1: Quasi-static estimation of lift coefficient

| $l_s/C$ | $\tilde{C}_L/(\tilde{l}/C)$ | Quasi-static estimation | Quasi-static model |
|---|---|---|---|
| 0.255 | ( 0.207, -0.0983) | ( 0.584, 0.0) | Figure 6(a), Equation (10) |
| 0.40 | ( 0.661, -0.451 ) | (0.580, -0.335) | Figure 6(b) , Equation (11) |
| 0.55 | (0.572, -0.344) | (0.580, -0.335) | Figure 6(b), Equation (11) |

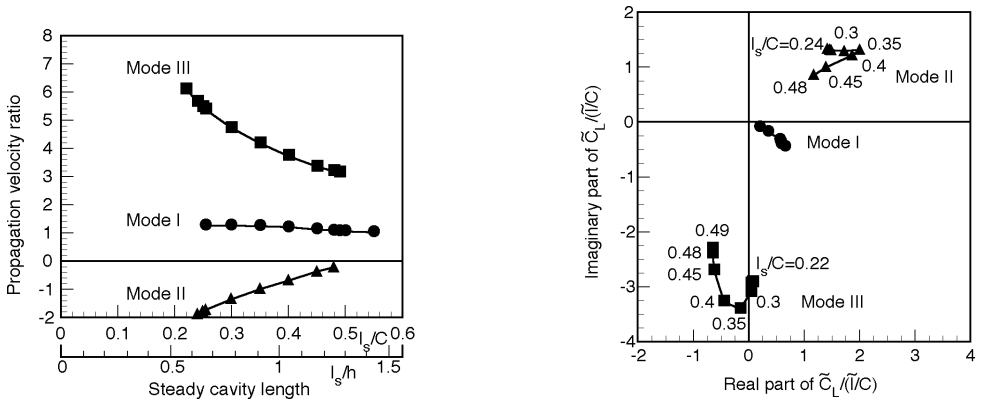


(a) Propagation velocity ratio (b) Unsteady lift coefficient

Figure 7: Propagation velocity ratio and unsteady lift coefficient for higher order modes.

$l_s/C$=0.255, a large discrepancy can be seen between the unsteady lift coefficient and the estimated value. This might be caused by the fact that the model does not consider the effect of the adjacent cavity for the case of shorter cavity. The relatively large frequency $|\omega_R|$ for this case may also cause this discrepancy.

### 3.4. Unsteady lift coefficients for higher order modes.

From Equation (4), we can obtain a lot of higher order modes in addition to the conventional rotating cavitation mode (Mode I). In this section, we focus on the other higher order modes, Mode II and III.

Figure 7 shows (a) the propagation velocity ratio $k_R^*$ of Mode I – III and (b) the unsteady lift coefficient per unit cavity length change $\tilde{C}_L/(\tilde{l}/C)$. From the propagation velocity ratio, we can see that Mode II and III correspond to the backward traveling rotating cavitation and higher order forward rotating cavitation, respectively. We can see from Figure 7 (b) that the magnitude of $\tilde{C}_L/(\tilde{l}/C)$ is larger for Mode II and III. Thus, we should pay more attention on higher order modes, while those are rarely observed in experiments.

### 3.5. Comparison with experiment

Figure 8 shows the pressure distributions on the blade surfaces obtained by the present analysis and the experiment (Maekawa et al., 1997) The parameters are set to be $C/h$=1.91, $\beta$=81.0[deg.] and $\alpha$=4.4[deg.]. The calculation is carried out in the neutrally stable condition with $l_s/C$=0.347. The magnitude of the cavity length fluctuation is assumed to be 30% of the steady cavity length. The experimental result is obtained from the pressure measurement on the casing wall. It is known from the visual observation that the low pressure region on the suction surface corresponds to the cavitating region. We can see not only from the numerical result but also from the experimental one that the pressure difference across the blade is larger in the cavitating region and the area of low pressure region fluctuates in accordance with the cavity length fluctuation. However, the magnitude is quite different from each other. This discrepancy is supposed to be caused by the linearization based on the assumption of small disturbances.

From the fact that the present calculation can simulate the tendency of the unsteady lift coefficient, we expect that the quasi-static model can predict the unsteady lift coefficient well if we obtain the steady lift coefficient $C_{LS}$ experimentally and utilize it for the quasi-static model. Further study should be conducted for the verification of the present model.

## 4. Concluding remarks

Results obtained by the present study can be summarized as follows.

(1) Mainly the pressure difference across the blade in the cavitating region is producing the lift on the blade.

(2) For the cases with shorter cavities where the cavity terminates outside of the blade passage, the pressure on the pressure surface does not fluctuate largely. Thus, the pressure fluctuation on the suction surface is essential for the unsteady lift coefficient.

(3) For the cases with longer cavities in which the cavity extends into the blade passage, the pressure on the pressure surface of the blade is affected by the cavity oscillation on the adjacent blade.

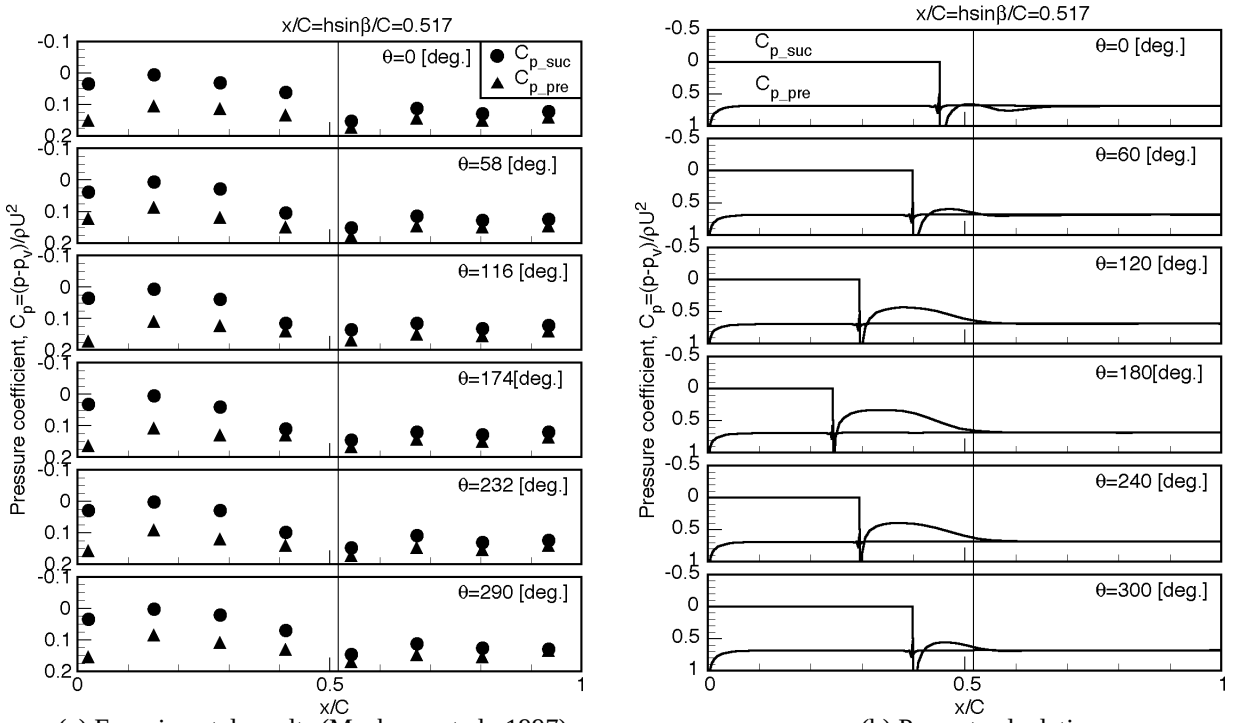


(a) Experimental results (Maekawa et al., 1997) (b) Present calculation

Figure 8: Comparison of temporal pressure distributions along blade surfaces between experiments and present calculation

(4) For the cases with longer cavities, the unsteady lift coefficient can be predicted quasi-statically by taking account of the effects of adjacent cavity.

(5) The unsteady fluid forces might be larger for the higher order modes than for the conventional rotating cavitation mode.

## Acknowledgments

This study is partly supported by the Grant-in-Aid from the Ministry of Education, Sports, Culture, Science and Technology.

## References

Furuya, O. (1982). *ASME Paper*, 147-155.

Kamijo, K., Yoshida, M. and Tsujimoto, Y. (1993). *AIAA J. Propulsion and Power*, **13**-4, 488-494.

Maekawa, M., Yoshida, Y., Tsujimoto, Y. and Kamijo, K. (1997). (in Japanese) *Trans. JSME, Ser.B*, **63**-605, 132-138.

Tsujimoto, Y., Kamijo, K. and Yoshida, Y. (1993). *ASME J. Fluids Engineering*, **115**-1, 135-141.

Tsujimoto Y., Yoshida, Y., Maekawa, Y., Watanabe, S. and Hashimoto, T. (1997). *ASME J. Fluids Engineering*, **119**-4, 775-781.

Watanabe, S., Sato, K., Tsujimoto, Y. and Kamijo, K. (1999). *ASME J. Fluids Engineering*, **121**-4, 834-840.